

Negative Index of Refraction in Optical Metamaterials

Vladimir M. Shalaev, Wenshan Cai, Uday Chettiar, Hsiao-Kuan Yuan, Andrey K. Sarychev*, Vladimir P. Drachev and Alexander V. Kildishev

School of Electrical & Computer Engineering, Purdue University, West Lafayette, IN 47907, USA

An array of pairs of parallel gold nanorods is shown to have a negative refractive index in the optical range, close to a wavelength of 1 μm . Such behaviour results from the plasmon resonance in the pairs of nanorods for both the electric and magnetic components of light. The metal rods act as inductive elements whereas the dielectric gaps perform as capacitive elements, forming an optical LC-circuit. Here we report both experiments and simulations that demonstrate a resonant behaviour for the index of refraction. Above the resonance, the refractive index becomes negative. Paired metal nanorods open new opportunities for developing negative-refraction materials in optics.

One of the most fundamental notions in optics is that of refractive index, which gives the factor by which the phase velocity of light is decreased in a material compared to vacuum conditions. Negative-index materials (NIMs) have a negative refractive index so that electromagnetic waves in such media propagate in a direction opposite to the flow of energy, which is indeed unusual and counterintuitive. There are no known naturally-occurring NIMs. However, artificially designed materials (metamaterials) that can act as NIMs have recently been proposed. Metamaterials can open new avenues to achieving unprecedented physical properties and functionality unattainable with naturally-existing materials. Proof-of-principle experiments¹ have shown that

* Present address: Ethertronics Inc., 9605 Scranton Road, Suite 850, San Diego, California 92121, USA.

metamaterials can act as NIMs at *microwave* wavelengths. NIMs drew a large amount of attention after Pendry predicted that NIMs with a refractive index $n = -1$ can act, at least in principle, as a ‘perfect lens’ allowing imaging resolution which is limited not by the wavelength but rather by material quality². Materials with structural units much smaller than the wavelength can be characterized by a dielectric permittivity $\varepsilon = \varepsilon' + i\varepsilon''$ and a magnetic permeability $\mu = \mu' + i\mu''$. In this case, the refractive index $n = \sqrt{\varepsilon\mu}$ becomes negative provided that the condition³ $\varepsilon''\mu' + \mu''\varepsilon' < 0$ is fulfilled. The condition $\varepsilon' < 0$ and $\mu' < 0$ is sufficient (but not necessary) for negative refraction⁴. In the latter case, light induces in the NIM an electric displacement and a magnetic induction, which are directed against the incident electric and magnetic fields, respectively.

NIMs with negative refraction in the optical range could have applications that are particularly spectacular, encompassing such areas as nanophotonics, nanolithography, and biomedical sensing and imaging. However, while negative permittivity in the optical range is easy to attain for metals, there is no magnetic response for naturally-occurring materials at such high frequencies. Two recent experiments employing lithographically-fabricated double and single split-ring resonators showed that a magnetic response and negative permeability can be accomplished in the terahertz⁵ and 100 terahertz⁶ spectral ranges. These experiments were a breakthrough in the field and showed the feasibility of NIMs in the optical range because a negative magnetic response is a precursor for negative refraction. However, the ultimate goal of negative refraction was not accomplished in either of these two important experiments. Below we report our observation of a negative refractive index for the optical range, specifically, for the wavelengths close to 1 μm (300 THz frequency). The NIM structural design we used closely follows our recent theoretical prediction of negative refraction in a layer of pairs of parallel metal nanorods^{7,8}.

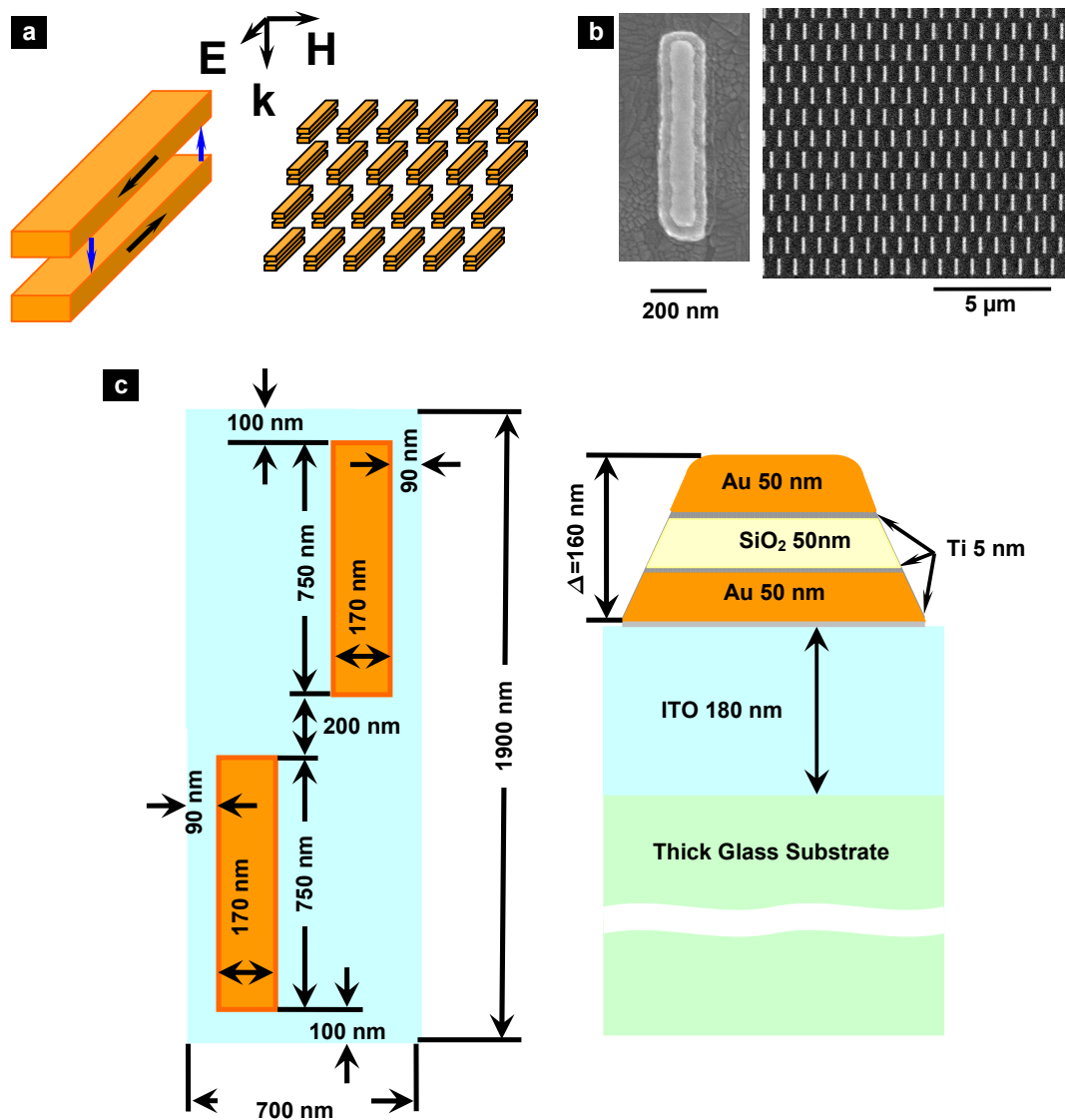


Figure 1 Pairs of parallel metal nanorods. **a**, A schematic for the array of parallel nanorods; the H-field induced current in the rods (black arrows) is closed by displacement current (blue arrows). **b**, Field-emission SEM picture (top view) of a single pair of gold nanorods (left) and a fragment of 2 mm \times 2 mm array of pairs of gold nanorods (right). **c**, Sizes of lower gold nanorods and their separations in the array (left) and a side-view schematic for one pair of nanorods on the substrate formed by an ITO layer and glass (right).

Figure 1a schematically shows the array of closely-spaced pairs of parallel metal nanorods used in our experiments. The two parallel rods form an open current loop, which acts as a transmission line and has a current resonance. Such a loop is ‘closed’ through the displacement current (blue arrows in Fig. 1a), and it therefore supports the resonant modes of both the electric and magnetic components of light. For normally-incident light with the electric field polarized along the rods and the magnetic field perpendicular to the pair, the electric and magnetic responses both can experience a resonant behaviour at certain frequencies that depend on the rod dimensions and their separations^{7,8}. In this design, the electric component of the incident wave excites a symmetric current mode in the two metal rods, whereas the magnetic field component excites an anti-symmetric mode (see Fig. 1a). The excitation of such plasmon resonances for both the electric and magnetic light components results in the resonant response of the refractive index, which can become negative above the resonance as previously predicted^{7,8}. This resonance can be thought of as a resonance in an optical LC-circuit, where the metal rods act as inductive elements L and the dielectric gaps between the rods act as capacitive elements C.

Experimental results were obtained using a 2 mm × 2 mm array of nanorods. Fig. 1b shows a field-emission scanning electron microscope (FE-SEM) image of a portion of the sample as well as a closer view of a single pair of rods. A schematic for the whole sample is given in Fig. 1c, and the details of manufacturing are described in the Methods section.

The optical characteristics of the periodic array of metal rods shown in Fig. 1a were simulated using a 3D finite difference time domain (FDTD) formulation, where the rectangular elementary cell of Fig. 1c represented the properties of the entire sample (for details, see the Methods section).

Figure 2 presents the results of our experimental measurements of transmittance (top), and reflectance (bottom) for light propagating through the sample and substrate described above. The scattering and diffraction of light for our sample was negligible. The transmission and reflection spectra are measured with a Lambda 950

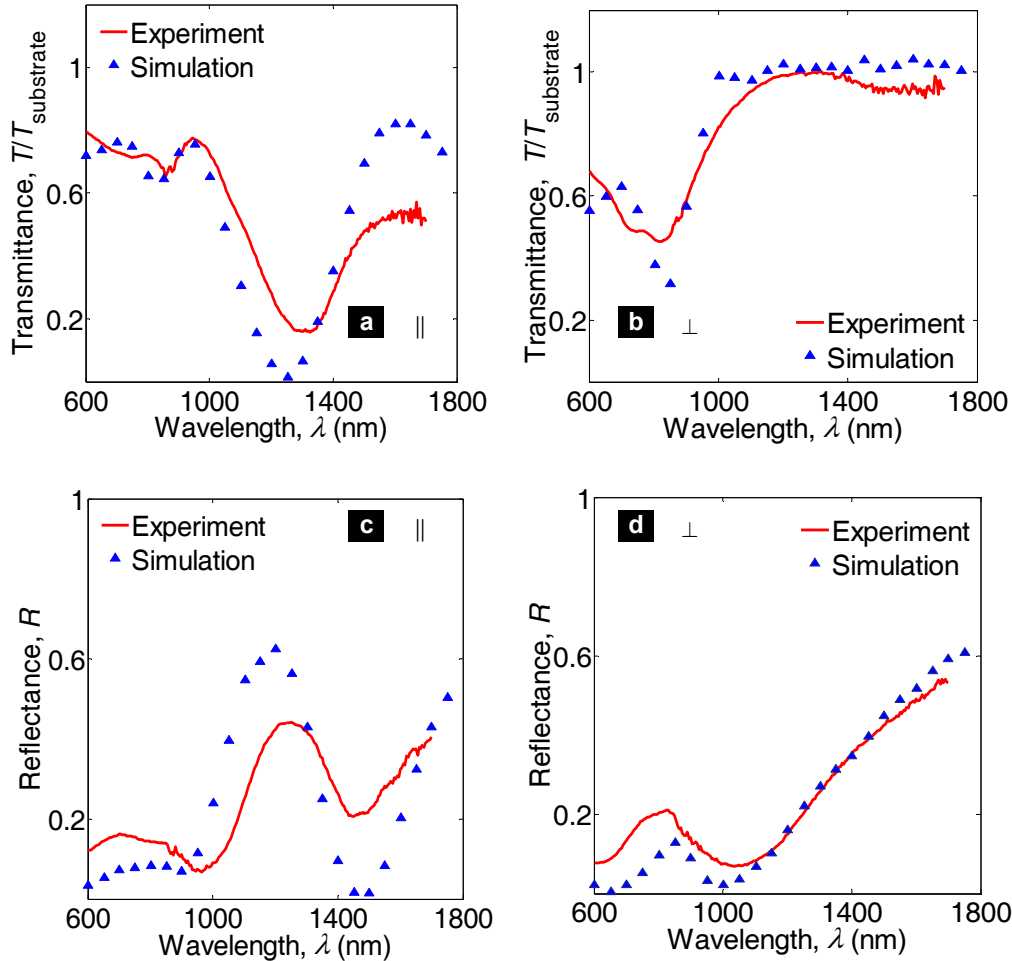


Figure 2 Transmittance T (a and b) and reflectance R (c and d) of light for the layer of pairs of parallel gold nanorods placed on a substrate of ITO-coated glass. Two different polarizations of light are used, one with the electric field along the rods (||), as in **a** and **c**, and one normal to the rods (perp), as in **b** and **d**. The transmittance of the whole sample is normalized by the transmittance of the substrate (ITO-coated glass) for both polarizations.

spectrophotometer from Perkin-Elmer using linearly polarized light. Two different light polarizations have been used, one with the electric field parallel (Figs. 2a and 2c) and the other with the electric field perpendicular (Figs. 2b and 2d) to the nanorod pair major axis. The transmission spectra are collected at normal incidence, and the reflection spectra are measured at a small incident angle of 8° . The divergence angle of the incident beam is up to $\sim 15^\circ$. The transmittance for the whole sample is normalized by the transmittance of the substrate for both light polarizations. The measured frequency dependence of the substrate formed by ITO-coated glass is described with very high precision by the Drude formula (see also Methods and Supplementary Information). The refractive index of glass is 1.5.

As seen in Fig. 2, the system of parallel gold nanorods shows a strong plasmonic resonance near $1.3 \mu\text{m}$ for light with the electric field polarized parallel to the rods. In this case, light excites both electric and magnetic responses such that the refractive index can become negative above the resonance. For light with the electrical field polarized perpendicular to the rods, only the electric (transverse) plasmon resonance is excited, with a resonant wavelength near 800 nm. The magnetic response is negligible in this case, and the refractive index is positive for all wavelengths.

We note good qualitative agreement between our 3D FDTD simulations and experimental data – both the positions and the widths of the resonances are reproduced well. The observed difference in magnitudes at some wavelengths is related to insufficient spatial resolution of the grid used in our simulations. The grid size in simulations was 10 nm; a higher resolution would be beyond the computational capabilities of available computers. Yet, for simulations of metals in the optical range, which is known to be a hard problem, the accomplished level of agreement is very good.

To investigate the negative refraction of our material, we also used polarization and walk-off interferometers. These interference methods are capable of revealing that the light phase is advanced in NIMs, rather than being delayed as in normal, positive-index materials. The results of these experiments are shown in Fig. 3. In the polarization interferometer, two optical channels have a common geometrical path and differ by the polarization of light. This allows one to measure the phase difference between orthogonally-polarized waves $\Delta\phi = \phi_{\parallel} - \phi_{\perp}$ caused by anisotropy of a refractive material. Note that the phase acquired in the substrate does not contribute to the phase difference $\Delta\phi$. The walk-off interferometer has two optical channels which differ in

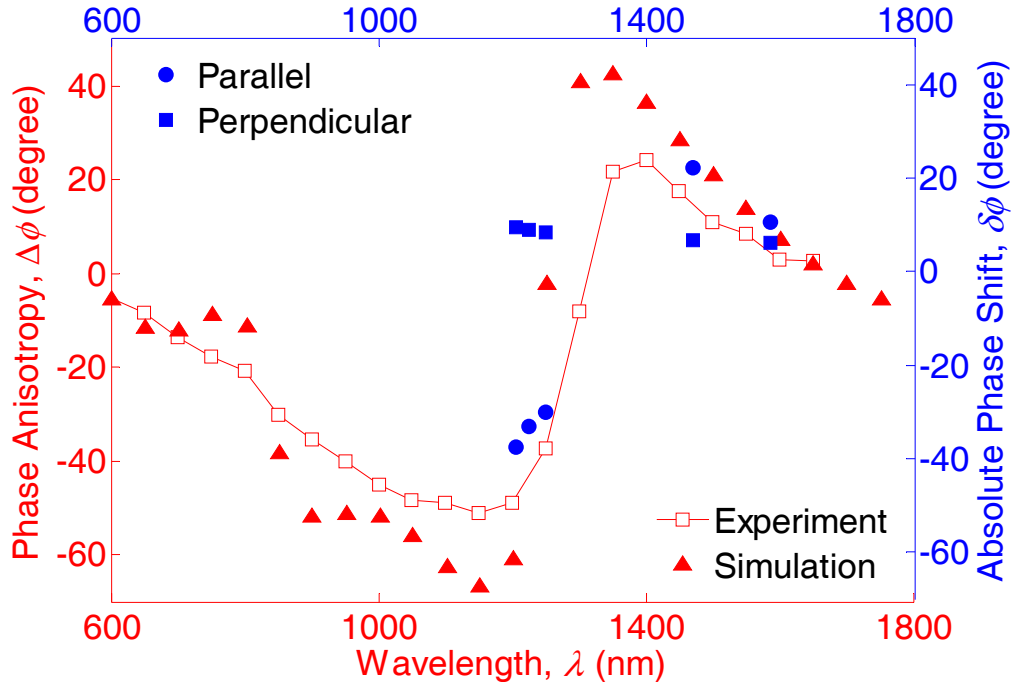


Figure 3 Phase change in the layer of pairs of gold rods for light polarized parallel and perpendicular to the rods. The measured (□) and simulated (▲) phase difference $\Delta\phi = \phi_{\parallel} - \phi_{\perp}$, for the parallel (ϕ_{\parallel}) and perpendicular (ϕ_{\perp}) polarizations (**left ordinate**). The absolute phase shifts $\delta\phi_{\parallel}$ and $\delta\phi_{\perp}$ for waves with parallel (●) and perpendicular (■) polarizations; the shifts are determined with respect to the layer of air of the same thickness as the layer of rods (**right ordinate**).

geometrical paths; it gives a phase shift introduced by a sample (ϕ_s) relative to a reference (ϕ_r): $\delta\phi = \phi_s - \phi_r$. The layer of air with the same thickness as the layer of rods was used as the reference. Both the reference and the sample beams go through ITO-coated glass used as the substrate so that the phase acquired in the substrate does not contribute to the measured phase shift $\delta\phi$ if the substrate has no variations in optical thickness. The walk-off effect in calcite crystals is employed to separate the two beams and then bring them together to produce interference. The phase shifts $\delta\phi_{\parallel}$ and $\delta\phi_{\perp}$ are measured for the two light polarizations, and their difference are compared with the phase anisotropy $\Delta\phi$ obtained from polarization interferometry (note that $\Delta\phi = \delta\phi_{\parallel} - \delta\phi_{\perp}$). The instrumental error of the phase anisotropy measurement by polarization interferometer is $\pm 1.7^\circ$. We note that variations in the substrate thickness do not affect the results of our phase anisotropy measurements, which is typical for common path interferometers. In the case of the walk-off interferometer, the thickness variation gives an additional source of error, causing an increase in the error for the absolute phase shift measurements up to $\pm 4^\circ$.

Figure 3 shows a very strong effect for our sample, with the phase difference $\Delta\phi = \phi_{\parallel} - \phi_{\perp} \approx -50^\circ$ at $\lambda \approx 1.2 \mu\text{m}$. As seen in Fig. 3, in the spectral range between 1 and $1.6 \mu\text{m}$ the absolute phase shift $\delta\phi_{\perp}$ measured with respect to the layer of air is positive and nearly flat (close to $+10^\circ$) in magnitude. This means that the refractive index is positive and light is delayed in this case. In contrast, $\delta\phi_{\parallel}$ shows a strong resonant dependence such that the difference $\delta\phi_{\parallel} - \delta\phi_{\perp}$ agrees very well with our measurements of $\Delta\phi$ using polarization interferometry. For $\lambda \approx 1.2 \mu\text{m}$, the phase advancement in the layer of nanorods with respect to the layer of air of the same thickness becomes very large ($\delta\phi_{\parallel} \approx -40^\circ$). For a material with a metal filling factor of only 8.3% and an overall structure thickness of about 165 nm, such phase advancement is indeed surprising and it indicates that the refractive index can be negative in this spectral range.

To find the refractive index we used Eq. (1) below, which provides the solution for retrieving the refractive index of a given thin layer of passive material ($\text{Im}(n) > 0$ and $\text{Re}(Z) > 0$, where Z is the impedance) with unknown parameters⁹. Specifically, we obtain the impedance (not shown here) and the refractive index of the equivalent homogeneous layer with the same complex reflectance r and transmittance t as the actual array of nanorods, without the ITO + glass substrate. (Note that the $T = |t|^2$ and $R = |r|^2$ shown in Fig. 2 are the power transmittance and reflectance, respectively.) Such a homogeneous layer with equivalent n and Z gives the same far-field distribution outside the sample as the actual layer of metamaterial.

The complex values of the reflected and transmitted electric fields, E_r and E_t , are calculated using 3D FDTD (see the Methods Section) for normally-incident light with electric field E_i . Then, $r = \alpha E_r(-d)/E_i(-d)$ and $t = \alpha E_t(d)/E_i(-d)$ are obtained from the field values, where $\alpha = \exp[ik(\Delta - 2d)]$, k is the wavenumber in air and d is the distance from the centre of the layer of the paired nanorods, with the total thickness $\Delta = 160$ nm, to the field evaluation planes in front and behind the sample. The distance d is chosen so that the reflected and transmitted waves (E_r and E_t) are plane waves with no more than 1% deviation in magnitudes in the evaluation planes. The index of refraction (n) of the nanorod layer is found from⁹:

$$\cos nk\Delta = \frac{1 - r^2 + t^2}{2t}. \quad (1)$$

In Fig. 4 we show the refractive index obtained using the above retrieval procedure for two light polarizations: electric field parallel (Fig. 4a) and perpendicular (the insert of Fig. 4a) to the nanorod pair major axis. Clearly, the index of refraction has a resonant behaviour for the parallel polarization, which enables the coupling of the structure to both the electric and magnetic field components of the light. To estimate the possible error of the inversion (Eq. (1)), the standard deviation (σ) of the refractive

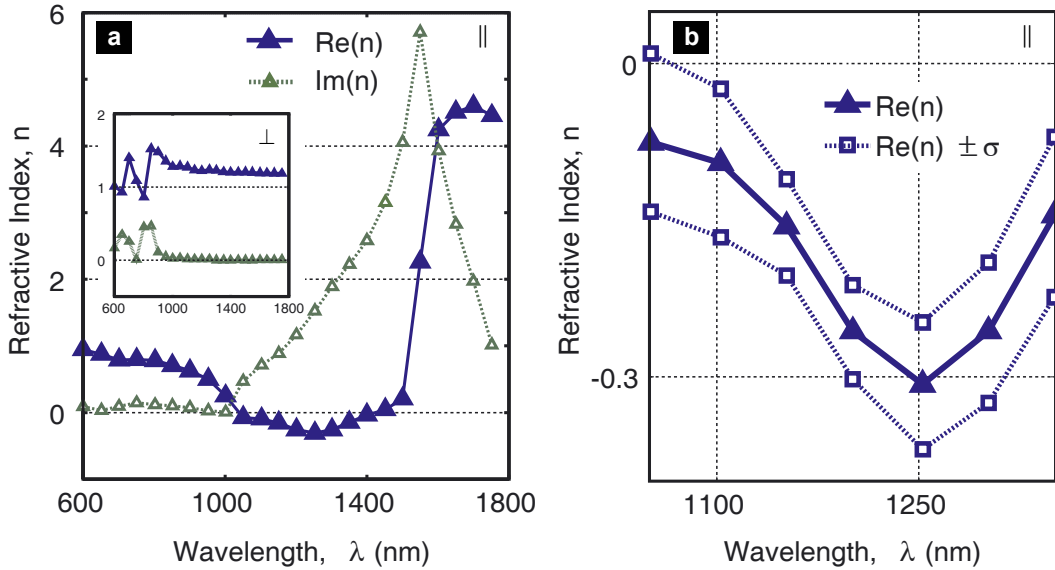


Figure 4 Real and imaginary parts of the refractive index for two orthogonal light polarizations. **a**, The main diagram shows the resonant behaviour of the refractive index for the polarization along the rods (\parallel). The insert in **a** depicts the refractive index for the polarization normal to the rods (\perp). **b**, The zoomed view of Fig. 4a for $\text{Re}(n) < 0$, including the upper and lower bounds with a one-sigma deviation.

index was found using the deviation of reflected and transmitted fields obtained at the evaluation planes. Figure 4b shows a closer view of the wavelength domain for negative n with upper and lower boundaries of $\text{Re}(n) \pm \sigma$. As seen in Fig. 4b, the effective refractive index is negative in the range between $1.1 \mu\text{m}$ and $1.4 \mu\text{m}$, reaching the magnitude $\text{Re}(n) \approx -0.3$ at $\lambda \approx 1.3 \mu\text{m}$.

For the perpendicular polarization, the magnetic response is negligible and the refractive index is always positive in this case (the insert of Fig. 4a). The two-peak structure in the insert can be explained by the interaction between the transverse plasmon oscillations in the two rods of a pair (the two overlapping peaks also can be traced in Figs. 2b and 2d).

We note that to introduce the effective dielectric permittivity $\epsilon(\omega)$ and magnetic permeability $\mu(\omega)$ depending only on frequency, the wavelength must be much larger than the dimensions of the elementary cell. This is not the case for our periodic structure of nanorods, where in general both μ and ϵ are tensors that depend on the quasi-wavevector \mathbf{k} . Accordingly, the effective-layer refractive index retrieved from Eq. (1) cannot be considered simply as the square root of the product of ϵ and μ . However, as mentioned above, the refractive index and the impedance for the effective NIM layer reproduce the electric and magnetic fields outside the actual sample exactly, and hence the use of these effective parameters is fully justified.

The relatively small magnitude of the negative refractive index obtained for our sample can indeed be enlarged by increasing the metal filling factor and by decreasing the separation of rods in the pairs^{7,8}. It is important to note that anomalously small refraction, $|n| \approx 0$, is also of great interest because it can result in interesting phenomena such as the beaming effect, which provides conversion of divergent light into a highly collimated beam.

The imaginary part of the refractive index also shows resonant behaviour and, for the parallel light polarization, it is rather large near the resonance. We note that by optimizing the system, losses can be significantly decreased. One of the possible ways to decrease losses is to fabricate structures much smaller than the wavelength so that the radiation loss would decrease. In accordance with this, loss is significantly lower for the perpendicular light polarization (Fig. 4b) because surface plasmon oscillations in this case occur along the smaller size (170 nm) of the system, normal to the nanorod major axis (note the smaller $\text{Im}(n)$ and the narrower resonance width in the inset of Fig. 4a). The magnetic response of parallel nanorod pairs can be accomplished even for structures much smaller than the wavelength, which means that negative refraction with

lower loss $\text{Im}(n)$ (and $\text{Re}(n) < -1$) can be obtained in this case¹⁰. Another possible way to decrease the effect of losses is to include an amplifying component into the NIM^{11, 12}.

In conclusion, for an array of pairs of parallel gold rods, we obtained a negative refractive index in the optical spectral range close to 1 μm . This is the first demonstration of negative refraction in the optical range. This new class of negative-index materials is relatively easy to fabricate on the nanoscale. The frequency for negative refraction depends on both the size of metal rods and their separation. The negative-refraction frequency can span the visible and near-infrared parts of the spectrum through appropriate nanorod array design. Further optimization of the proposed structures would allow NIMs with lower losses and larger magnitudes of negative refraction, resulting in new applications based on this unique phenomenon.

Methods

Sample fabrication. A 2 mm \times 2 mm array of nanorods was fabricated on a 180-nm layer of indium tin oxide (ITO) coated onto glass. Before applying the photo-resist for electron beam writing, the ITO-coated glass substrate was cleaned and baked at 160°C for 30 minutes. Next, a double layer of PMMA photo-resist was coated onto the ITO-glass substrate. A JEOL JBX-6000FS electron beam writer with optimized dosage was used for writing. After the photo-resist was developed, the desired sandwich structure of metal rods and silicon dioxide (SiO_2) was deposited in an electron beam evaporator at high vacuum. The thickness and sequence of the sandwich structure on the ITO-glass substrate are as follows: 5 nm of titanium (Ti), 50 nm of gold (Au), 5 nm of Ti, 50 nm of SiO_2 , 5 nm of Ti and finally 50 nm of Au. A lift-off process was then performed to obtain the array of paired nanorods.

The fabrication resulted in rods that were trapezoidal in shape (with a top-down width difference of 20 nm for each rod) and had the sizes and separations specified in

Fig. 1c. Figure 1c shows the sizes ($750 \text{ nm} \times 170 \text{ nm}$) of the bottom rods; the top rods are different in size and are $670 \text{ nm} \times 90 \text{ nm}$. This size difference is clearly seen in Fig. 1b for the single rod pair.

Simulation techniques. The core FDTD techniques have all been published extensively¹³. Our modelling was mainly focused on adequate integration of frequency-dependent permittivity in the general 3D FDTD evolution equation. To simulate the permittivity, the matching Debye models were obtained from the Drude models for the gold nanorods, $\varepsilon_{\text{Au}} = 9.0 - (1.3673 \times 10^{16})^2 / [\omega^2 + i(1.0027 \times 10^{14})\omega]$ and ITO, $\varepsilon_{\text{ITO}} = 3.4626 - (2.9134 \times 10^{15})^2 / [\omega^2 + i(1.5030 \times 10^{14})\omega]$, where $\omega = 2\pi c / \lambda$ (see Supplementary Information).

We set an elementary cell with $x \times y \times z = 1900 \text{ nm} \times 700 \text{ nm} \times 4000 \text{ nm}$ illuminated by a monochromatic plane wave at normal incidence. The overall geometry of the nanorods inside the elementary cell followed the trapezoidal shape of the experimental sample. Since we used a uniform grid with a spatial resolution of 10 nm, the 5-nm Ti layers (Fig. 1c) were not taken into account in those simulations. The thick glass layer was considered infinite in the simulations with the substrate of ITO-coated glass (Fig. 2). The results in Fig. 4 were obtained using exactly the same elementary cell, but without the ITO-glass substrate. Two perfectly matching layers¹³, which emulate infinite propagation of the scattered field, were arranged in front of and behind the nanorods. Standard periodic boundary conditions were applied to the elementary cell elsewhere to ensure periodicity of the entire array. The total-scattered field separation technique was used to obtain the scattered fields¹³. The field data for reflection and transmission coefficients were taken at selected evaluation planes in front of and behind the nanostructure using one-period sampling and additional Fourier filtering with averaging over the evaluation planes.

Received

References

1. Shelby, R. A., Smith, D. R., & Schultz, S. Experimental Verification of a Negative Index of Refraction. *Science* **292**, 77 (2001).
2. Pendry, J. B. Negative refraction makes a perfect lens. *Phys. Rev. Lett.* **85**, 3966 (2000).
3. Depine, R. A. Lakhtakia, A. A new condition to identify isotropic dielectric-magnetic materials displaying negative phase velocity. *Microwave and Optical Technology Letters* **41**, 315 (2004).
4. Veselago, V. G. The electrodynamics of substances with simultaneously negative values of permittivity and permeability. *Sov. Phys. Usp.* **10**, 509 (1968).
5. Yen, T. J. *et al.* Terahertz magnetic response from artificial materials. *Science* **303**, 1494 (2004).
6. Linden, S. *et al.* Magnetic response of metamaterials at 100 terahertz. *Science* **306**, 1351 (2004).
7. Podolskiy, V. A., Sarychev, A. K. & Shalaev, V. M. Plasmon modes in metal nanowires and left-handed materials. *J. of Nonlinear Opt. Physics and Materials* **11**, 65 (2002)
8. Podolskiy, V. A., Sarychev, A. K. & Shalaev, V. M. Plasmon modes and negative refraction in metal nanowire composites. *Optics Express* **11**, 735 (2003).
9. Smith, D. R., Schultz, S., Markoš, P. & Soukoulis, C. M. Determination of effective permittivity and permeability of metamaterials from reflection and transmission coefficients. *Phys. Rev. B* **65**, 195104 (2002).
10. Sarychev, A. K. & Shalaev, V. M. Magnetic resonance in metal nanoantennas. *SPIE Proceedings* **5508**, 128 (2004).

11. Ramakrishna, S. A. & Pendry, J. B. Removal of absorption and increase in resolution in a near-field lens via optical gain. *Phys. Rev. B* **67**, 201101(R) (2003).
12. Lawandy, N. M. Localized surface plasmon singularities in amplifying media. *Appl. Physics Lett.* **85** 5040 (2004).
13. Taflove, A. & Hagness, S. *Computational Electrodynamics: The Finite-Difference Time-Domain Method* (Artech, Boston, MA, 2000).

Acknowledgements

This work was supported in part by NSF-NIRT award ECS-0210445 and by ARO grant W911NF-04-1-0350.

Correspondence and requests for materials should be addressed to V. M. S. (e-mail: shalaev@purdue.edu).

Competing financial interests

The authors declare that they have no competing financial interests.

Supplementary Information

Transmittance and reflectance of ITO-coated substrate

To model optical properties of the ITO-coated substrate used in our experiments, the

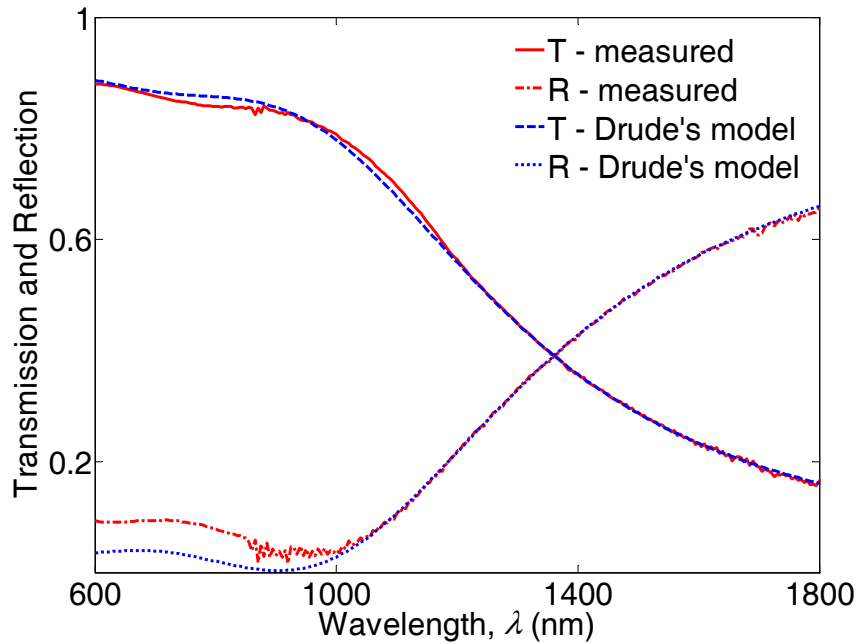


Figure S1 Transmission (T) and reflection (R) spectra of the ITO-coated glass.

following Drude formula was applied

$$\varepsilon = (n' + in'')^2 = \varepsilon' + i\varepsilon'' = 3.4626 - \frac{(2.9134 \times 10^{15})^2}{\omega^2 + i(1.5030 \times 10^{14})\omega}, \quad (S1)$$

where $\omega = 2\pi c / \lambda$, $n' = \text{Re}(n)$, and $n'' = \text{Im}(n)$. The ITO glass for our sample is CG-411N from Delta Technologies with a thickness of 180 nm. In Fig. S1 the measured transmission and reflection of our ITO-coated glass are compared against the calculated values using the Drude model (S1). There is excellent agreement between the measured and calculated values as seen in Fig. S1.